chemosensors

Article

A Method of Ultra-Low Power Consumption Implementation for MEMS Gas Sensors

Yu Bing [1], Fuyun Zhang [1], Jiatong Han [1], Tingting Zhou [1], Haixia Mei [1,2,3,*] and Tong Zhang [1,*]

[1] State Key Laboratory of Integrated Optoelectronics, College of Electronic Science and Engineering, Jilin University, Changchun 130012, China
[2] College of Automotive Engineering, Jilin University, Changchun 130021, China
[3] College of Electronic Information Engineering, Changchun University, Changchun 130022, China
* Correspondence: meihaixia1985@163.com (H.M.); zhangtong@jlu.edu.cn (T.Z.)

Abstract: In recent years, there has been a growing need for the development of low-power gas sensors. This paper proposes pulse heating and a corresponding measurement strategy using a Pulse Width Modulation (PWM) signal to realize the ultra-low power consumption for metal oxide semiconductor (MOS) gas sensors. A Micro-Hot-Plate (MHP) substrate was chosen to investigate the temperature and power characteristics of the MHP under different applied heating methods. The temperature of this given substrate could respond to the applied voltage within 0.1 s, proving the prac ticability of a pulse heating strategy. In addition, Pd-doped SnO_2 was synthesized as the sensing material in the implementation of an ultra-low power gas sensor. The sensing performance and power consumption under different conditions were compared in the detection of reducing gases such as ethanol (C_2H_5OH) and formaldehyde (HCHO). Additionally, the results revealed that the sensor could work under PWM excitation while reducing the operating power to less than 1mW. The features shown in the measurements provide the feasibility for MOS gas sensors' application in wearable and portable devices.

Keywords: ultra-low power; PWM excitation; Micro-Hot-Plate; MEMS; gas sensors

Citation: Bing, Y.; Zhang, F.; Han, J.; Zhou, T.; Mei, H.; Zhang, T. A Method of Ultra-Low Power Consumption Implementation for MEMS Gas Sensors. *Chemosensors* **2023**, *11*, 236. https://doi.org/10.3390/chemosensors11040236

Academic Editor: Pi-Guey Su

Received: 10 March 2023
Revised: 4 April 2023
Accepted: 5 April 2023
Published: 10 April 2023

1. Introduction

As the most important component in gas detecting equipment, gas sensors are widely used in environmental monitoring and gas leakage detection [1,2]. Among all the gas sensors, chemical gas sensors based on MOS material are widely studied and applied [3,4]. Recently, with the growing popularity of the Internet of Things (IOT), a new generation of gas sensors requires more characteristics such as portability and low power consumption. However, MOS gas sensors usually need to work at high operating temperatures, thus leading to considerable power consumption.

Numerous attempts in different aspects have been made to lower the power consumption of gas sensors. First of all, diverse microstructures have been built to reduce the operating temperature of the sensing material [5,6]. A reported manganese-doped ZnO sphere material was developed for NH_3 sensing that could work at 150 °C with a sensitivity of 28.5 [7]. Additionally, some materials with special structures could even show an obvious response at room temperature [8,9]. It is worth noting that the reduction in a sensor's operating temperature is only feasible for several types of target gases through improvements in their material and morphology.

At the same time, many researchers have been working on the improvement of the sensor's structure to cut down energy consumption. Traditional gas sensors based on cylindrical ceramic tubes using spiral heating wires are power greedy and usually need up to 1 W [10–12]. Typical flat gas sensors with a thin film structure often have platinum 45-made heaters as well as electrodes on either side of the insulating substrate; these miniature devices have a heating consumption power of 80–100 mW [13,14]. Owing to the continuous

development of advanced manufacturing, the IC technique on silicon has enabled the fabrication of ultra-compact sensor substrates. Sensors using these substrates are also known as Micro-Electro-Mechanical System (MEMS) gas sensors.

The silicon-based substrates used in these sensors are highly integrated with multilayer structures, which usually consist of a micro-heater, an interdigital electrode, and insulation layers [15]. Benefiting from the manufacturing processes and the ultra-compact structures, these sensors commonly have better uniformity [16] and lower power consumption [17,18]. Compared to traditional chemical gas sensors based on a ceramic tube structure and flat ceramic substrate, sensors with micro-heaters could reduce power consumption to around 30 mW [19–22]. However, the reduction in MHP's dimension has a limitation. Heating strategies need to be improved to further cut down the power consumption of MEMS gas sensors.

Therefore, in this work, pulse heating and the corresponding resistance signal sampling method were employed to realize ultra-low power consumption by cutting down the average heating duration. In order to explore the operating parameters, a measuring system was built to investigate the characteristics of MHP's temperature and power consumption under different conditions. These characteristics are used to figure out the heating parameters of the pulse heating voltage. In addition, a gas sensor was fabricated on an MHP substrate as an implementation of a low-power sensing strategy using synthesized Pd-doped SnO_2 as the sensing material, which is suitable for the detection of reductive gases [23–26]. Using ethanol vapor as the target gas, experiments were carried out aiming at sensing performance as well as power consumption, which could prove the feasibility of the heating strategy adopting PWM voltage signals.

This heating and measuring method could realize adjustable power consumption in gas sensing using MHP gas sensors and keeping the sensing performance while easily reducing the heating power to less than 1 mW. The sensing performance suggests that the pulse heating method provides the ability for MOS gas sensors to be used in portable and low-power devices.

2. Basis for the Ultra-Low Power Consumption Method

2.1. The Excitation and Measuring System

An excitation and measuring system was designed in this work, aiming at the dynamic temperature and resistance value of ultra-low power consumption MEMS gas sensors. The architecture of the system is portrayed in Figure 1. To implement this system, the ESP32 microcontroller was chosen to be used as the controlling unit due to its embedded Digital to Analog Converter (DAC) and Bluetooth module, which provided us with the necessary features and flexibility for our experiments. Specifically, the DAC output pin was used to provide the MHP's heating voltage. To ensure a relatively high output current, a voltage follower was incorporated into the corresponding peripheral circuit. Additionally, to eliminate high-frequency noise while maintaining the waveform of the heating voltage pulse signal, a low-pass filter was utilized, and its circuit parameters were adjusted accordingly (see the corresponding peripheral circuit in Figure S1).

In the DC excitation mode, a stable voltage was applied to the heating electrodes of the MHP sensor. This stable voltage ensured that the temperature of the sensing material remained constant, and the resistance values of the sensing material were sampled at a stable rate through the signal electrodes. In the pulse heating mode, the PWM heating voltage was applied to the MHP sensor. The pulse width was adjusted to control the heating duration, and the voltage value was adjusted to control the maximum temperature of the sensing material. After each heating duration, the sensing material's resistance values were measured. These resistance values were then processed and used as the output data for gas detection.

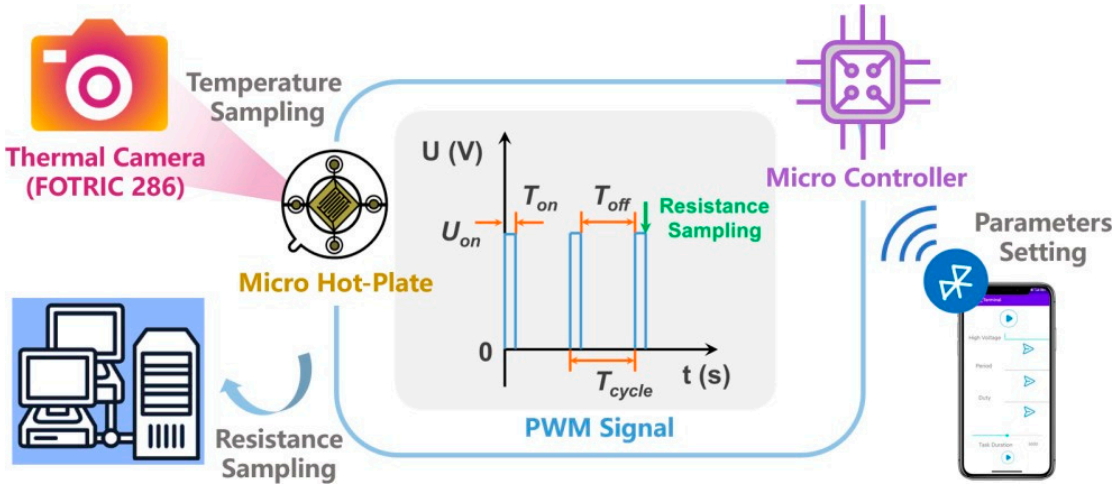

Figure 1. The measuring system for MEMS gas sensors.

Owing to the DAC's adjustable voltage output ability, the system incorporated wireless communication to realize the programmable control of the heating voltage. Specifically, it included several parameters of the applied PWM voltage that is shown in Figure 1, such as the heating voltage (U_{on}), the cycle's length (T_{cycle}), and the duty ratio, which is defined by T_{on}/T_{cycle}. These parameters could be regulated through a Bluetooth communication module in the microcontroller using a mobile phone, enabling the convenient control of the sensor's operating temperature.

In addition, the temperature value sequences used in this experiment were captured by a thermal camera (FOTRIC 286), which had a spatial resolution of 1.14 mrad and a range of temperature measurements from −40 °C to 700 °C. These parameters could satisfy the need for the dynamic temperature sampling of MHP. An electrochemical workstation (CHI660E) was used to realize the accurate measurement of the heater's resistance.

Experiments have been carried out to investigate MHP's temperature properties shown under different heating methods, and the power consumption under different conditions has been calculated and used in the modulation of MHP's heating duration. Additionally, the MHP (typed GS-3000, Figure S2) we used in this experiment was purchased from the Company of MEMS Sensor and Technology (Suzhou, China).

The temperature of MHP's surface could reach a certain value after the heating voltage was applied to the electrodes, thus providing an optimal operating condition for the sensing material and allowing the sensor to show a clear response. (The discussion of the sensing mechanism is given in Section 3.3) As MHP heated up, its infrared radiation signal was captured by a thermal camera, which then exported the data to the PC terminal through the Universal Serial Bus (USB) interface. During this process, the resistance value of the sensing material was sampled at the end of each T_{on}, which was realized by the regulation of the Analog to Digital Converter (ADC)'s sampling rate and the timer's interrupt request in the program's control logic. The acquired data were then used in processing and analysis to evaluate the gas sensing performance.

2.2. Fast Temperature Response of the MHP

The temperature values that MHP's surface reached under different heating voltages were put under comparison. The heating duration T_{on} was set to 1 s and 0.1 s with the heating voltage U_{on} of 1 V and 2 V, respectively. Those voltage cycles with the T_{on} of 1 s could provide MHP with a stable temperature, which is considered the same value as the DC excitation. As the curve in Figure 2a has illustrated, the micro heater could reach the same temperature as the steady-state under DC excitation within the voltage's exerting time of 0.1 s. Additionally, this temperature could be held when T_{on} > 0.1 s.

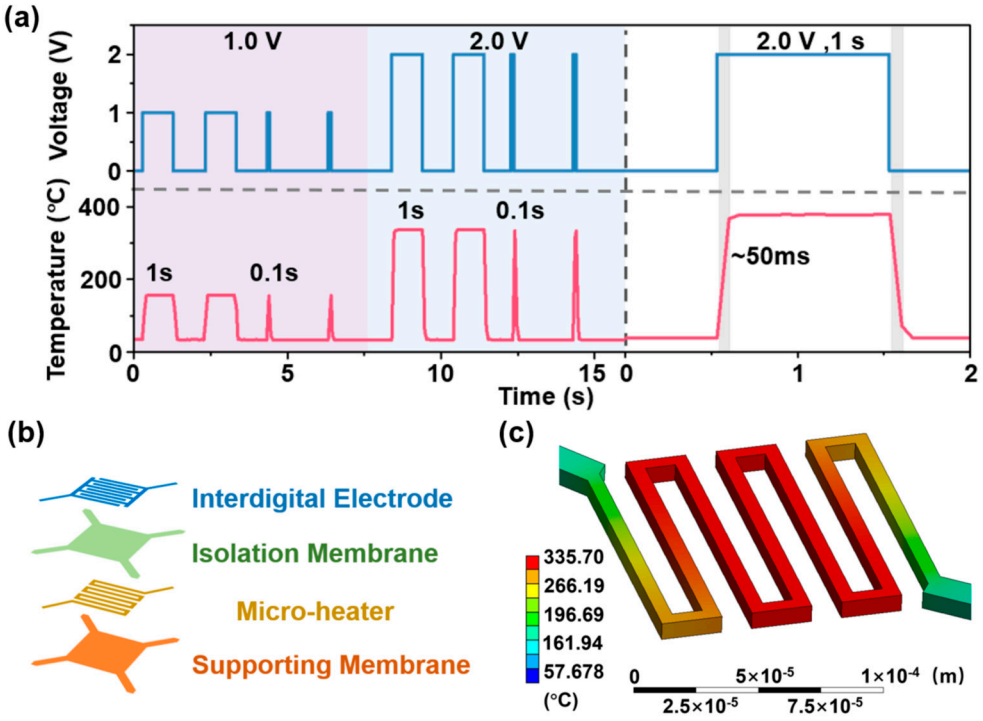

Figure 2. (**a**) The temperature variation in the MHP's surface under different heating voltage. (**b**) The schematic diagram of the MHP' s four-layer structure. (**c**) The temperature distribution of the MHP by finite element analysis under 2.0 V.

Additionally, the temperature variation in the magnified cycle pictured the temperature response when a 2.0 V heating voltage was applied on the heating electrodes and removed after 1 s; the surface temperature of the sensor's substrate could reach the maximum value within 50 ms, and the device could maintain the operating temperature until the moment when the applied voltage was removed. Those revealed properties indicate that the micro heater could be driven by the PWM method, and the heating voltage could last more than 0.1 s.

At the same time, finite-element analysis was used to study the temperature distribution and dynamic temperature response of the microheater under a cycling operating voltage. Some parameters involving the structure and materials' properties were set to perform the simulation. As is shown in Figure 2b, the MEMS-based gas sensing device had a four-layer structure. A Si_3N_4 layer was grown on the SiO_2 substrate, which acted as a supporting membrane and provided mechanical support. The micro heater was made of platinum, titanium, and tungsten and had a resistance of 40 Ω at room temperature. A 300 nm isolation membrane made of Si_3N_4 was used between the electrodes and the micro-heater layer. A pair of interdigital electrodes were placed on the top layer of the MHP as the signal electrodes of sensing materials.

The infrared emission coefficient of the MHP was set at 0.3, which was the same value used in the temperature measurement. The temperature distribution of the MHP under 2.0 V is shown in Figure 2c. Additionally, the dynamic variation in the micro heater's temperature is given in the supporting information, illustrating the quick temperature response of the sensor's substrate.

2.3. Power Characteristics

In the meantime, multiple measurements were carried out in order to reveal the power performance of the MHP. First of all, the temperature of the MHP's working area under different applied DC voltages was measured in the experiment. Additionally, the fitting results of the data revealed a linear relationship between MHP's temperature and the

corresponding voltage, which is illustrated in Figure 3a. This relationship indicates that the temperature of the MHP's surface could be determined by the given voltage value, and it allowed for accurate temperature control and maintenance, which is essential for maximizing the device's efficiency.

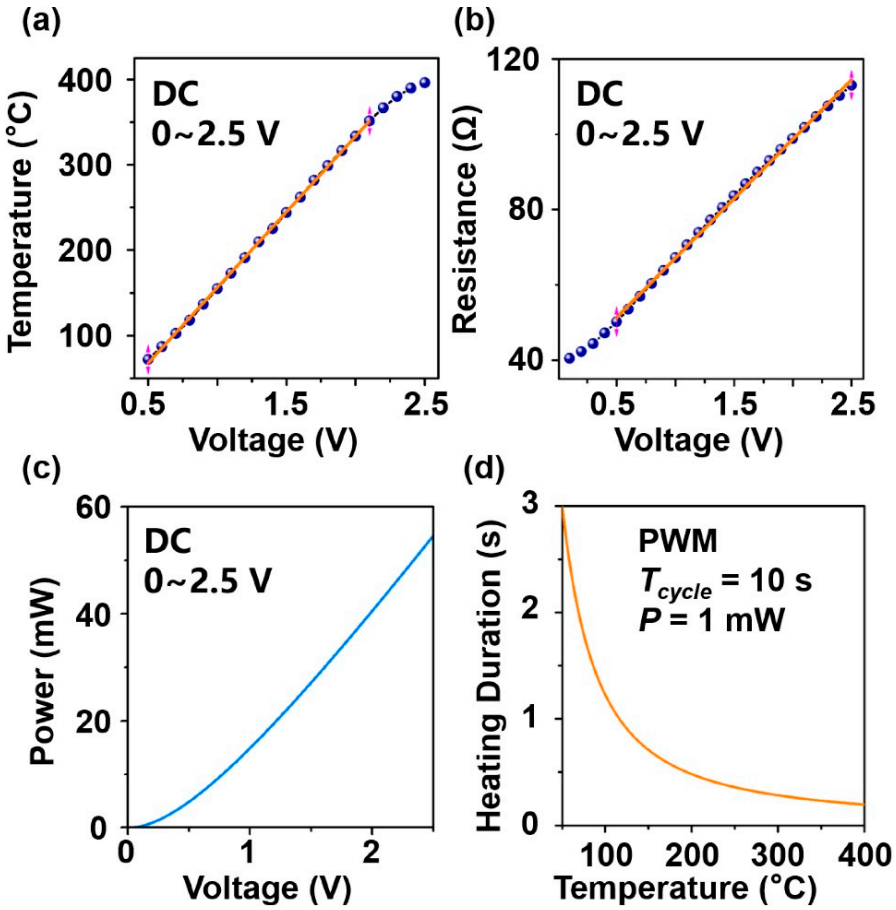

Figure 3. (**a**) The temperature variation in the MHP with applied DC voltage (**b**) The resistance of the micro-heater under different applied DC voltages (**c**) The power consumption of the micro-heater under different applied DC voltages (**d**) The maximum heating duration (T_{on}) when T_{cycle} = 10 s, p = 1 mW.

In addition, for the micro-heater, a metal material similar to platinum has a resistance that varies with the temperature according to the following rule when the temperature is less than 600 °C, where α is the temperature coefficient of resistance (TCR), R and R_0 represent the resistance at the temperature of T and room temperature, respectively.

$$R = R_0 (1 + \alpha T) \quad (1)$$

The microheater's resistance dynamic variation with temperature was measured by the electrochemical workstation's i-t mode when the applied DC voltage (U) changed from 0 to 2.5 V, which was linearly dependent, as is shown in Figure 3b. The fitting result is given where $R = 31.58 \cdot U + 35.53$, each resistance value was used as a correction of the estimated power consumption, and the final relation between power under DC excitation (P_{dc}) and the applied voltage can be described as follows, while the corresponding curve is pictured in Figure 3c.

$$P_{dc} = U2/R = U2/(31.58U + 35.53) \quad (2)$$

Therefore, the heating power under PWM excitation (P) could be estimated using the given parameters $P = P_{dc} \times T_{on}/T_{cycle}$.

Aiming at MHP's ultra-low power consumption, the heating power was limited to 1 mW. The maximum heating duration (T_{on}) in each cycle was derived from the estimated power expression given in the 10 s' PWM cycle and the relationship between T_{on} and the target power consumption. Once the maximum heating duration was determined, it could be used in the PWM excitation method for any given sensing material with a definite operating temperature. This meant that the maximum heating duration could be estimated for each sensing material based on the relationship shown in Figure 3d.

Overall, the process of aiming at ultra-low power consumption in the MHP involved the consideration of power restrictions and the operating characteristics of the sensing material. By using the maximum heating duration derived from the estimated power expression and the PWM excitation method, it was possible to optimize the performance of the MHP while minimizing power consumption.

3. Verification and Discussion

3.1. The Fabrication of the Gas Sensor

As a verification of the proposed heating and measuring method aimed at low power consumption, a gas sensor with an MHP substrate was fabricated and adopted. The sensing material Pd-doped SnO_2 was prepared by the sol-gel method, which is suitable for large-scale production.

The synthesis process is pictured in Figure 4. First of all, a 10 g $SnCl_4 \cdot 5H_2O$ sample was dissolved in 40 mL of deionized water under magnetic stirring. In order to facilitate the hydrolysis process, an $NH_3 \cdot H_2O$ solution (volume ratio, ammonia: deionized water = 1:1 and 1:4) was slowly added to the solution. The pH was titrated to 4 for the sol's formation. After being washed with deionized water at 60 °C, the milky white precipitate was dried in an electric air oven for 5 h to remove the solvent component. Then, calcination was performed in a tubular muffle furnace for 2 h at 600 °C to drive off the water molecules and residues from the desired sample and obtain the SnO_2 powder.

Figure 4. Schematic diagram of the formation of Pd-doped SnO_2 MEMS gas sensor.

To realize the doping of palladium, the $PdCl_2$ powder was mixed with SnO_2 (one percent mass ratio, 0.01g $PdCl_2$, and 1 g SnO_2) in deionized water under uniform stirring for 2 h, and the mixture was dried in an electric air oven in succession. Lastly, the final Pd-doped SnO_2 sample was obtained by 600 °C calcination in the tubular muffle furnace for 2 h.

The synthesized 1% Pd-doped SnO_2 was used as the sensing material, which was applied on the MHP substrate through drop coating. Meanwhile, a traditional ceramic tube sensor was fabricated as a contrast using the same sensing material.

The morphologies of the prepared Pd-doped SnO_2 particles were investigated through scanning electron microscopy (SEM), with the corresponding image shown in Figure 5a, which proved that the nanoparticles' diameters were approximately 20–30 nm. In addition, the XRD pattern of the material is given in Figure 5b, where the diffraction peaks match well with the cassiterite crystal phase SnO_2 with a tetragonal rutile structure (JCPDS 41-1445). Several peaks with the index of (110), (101), and (200) are marked in the pattern.

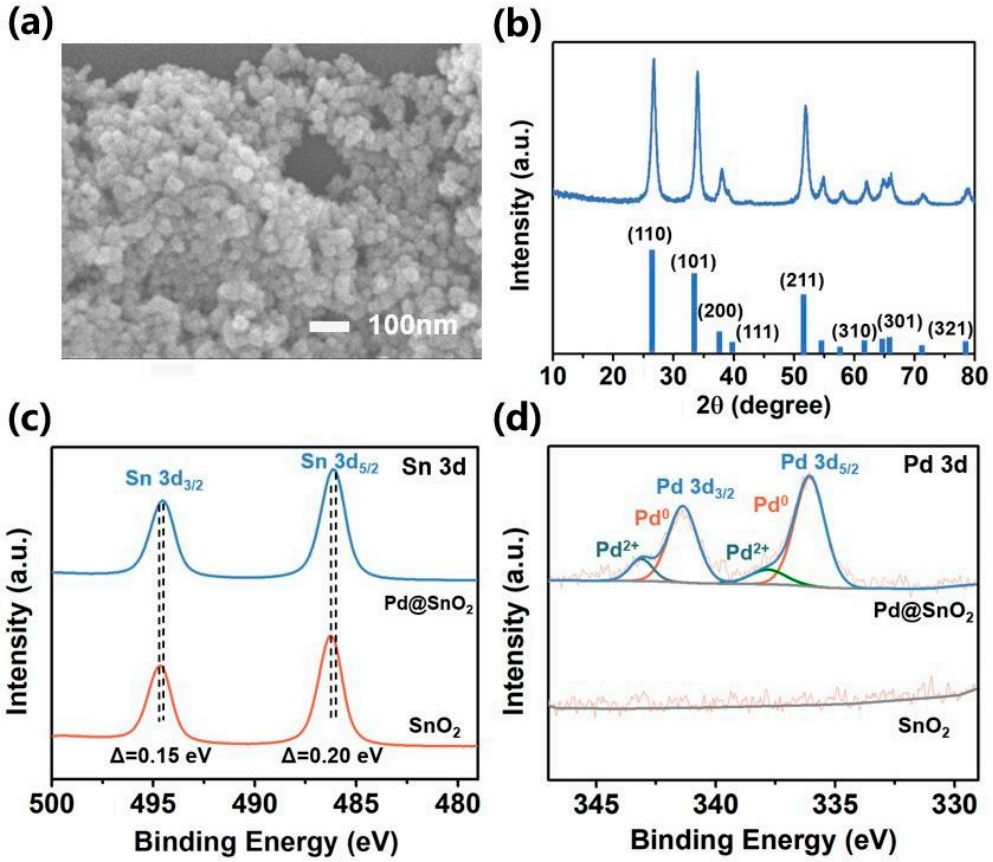

Figure 5. (**a**) SEM image (**b**) XRD pattern (**c**) XPS Sn 3d and (**d**) XPS Pd 3d of the prepared Pd-doped SnO_2 particles.

Furthermore, X-ray photoelectron spectroscopy (XPS) was carried out to evaluate the chemical state of the prepared material (Figure 5c,d). The Sn^{4+} $3d_{3/2}$ (494.68 eV) and Sn^{4+} $3d_{5/2}$ (486.28 eV) peaks are shown in the pure SnO_2 (Figure 5c), and the corresponding peaks of the Pd-doped SnO_2 are 494.53 eV and 468.08 eV. The Pd 3d spectra prove the existence of the Pd nanoparticles as a dopant, and two peaks are decomposed into two parts (Figure 5d). These peaks indicate that the Pd molecules mainly consisted of Pd^0 (84.22%) and Pd^{2+} (15.78%) [27].

3.2. Gas Sensing Properties

Furthermore, the excitation method mentioned above was implemented on this MHP, with ethanol vapor chosen as the target gas to demonstrate the sensing performance. The operating resistance and dynamic response-recovery curve of the fabricated sensors toward ethanol vapor were measured using the excitation and measuring system established in Section 2.1.

To ensure the stability of the material's sensing performance, the sensor was put under a 2.0 V DC voltage (around 330 °C) for 8 h before testing. The measured optimum operating temperature of the sensing material was tested to be around 260 °C, with the corresponding experiment results given in Figure S3.

The power consumption, as well as the sensing performance of the proposed gas sensing material using different substrates under different heating methods, were put under comparison. The heating power was provided by a constant current source. The MHP sensor under DC excitation was heated by a constant voltage of 1.6 V, which could provide a temperature of 260 °C for the sensing material. According to the temperature properties and power estimation explored in the experiments (Sections 2.2 and 2.3), for the MHP sensor adopting the PWM heating strategy, the heating voltage (U_{on}) in each cycle was set to the same value as that in the DC heating method, which was 1.6 V.

To find a balance between the sensing performance and the power consumption, the heating power was restricted to 1 mW, which is an ultra-low power consumption level for MEMS gas sensors. To cover the temperature response time of the MHP and ensure the accumulation of active oxygen, the sensor needed a minimum heating duration of several hundred milliseconds. On the other hand, a longer pulse cycle time would inevitably lead to an extension of the response and recovery times. Taking these factors into consideration, the heating duration and the pulse cycle time were set at 0.32 s and 10 s, respectively, using the power properties given in Figure 3c,d. Subsequent experiments have proved that these parameter settings can meet the sensor's use within the common ethanol detection range.

Figure 6a provides the detailed output resistance value of the MHP gas sensor on exposure to 100 ppm of ethanol under the PWM excitation method (as shown in Figure 6c), with the enlarged view of the sensor's response stage given in Figure 6b. According to the resistance sampling method proposed in Section 2.1, the resistance signal sampled at the end of each U_{on} (Figure 6d) was used as the resistance value in the response–recovery curve (Figure 6e). Additionally, the response–recovery curve and its corresponding resistance value were then used to evaluate the sensing performance. As a comparison, the variation in sensor resistance upon the application of voltage was measured, and the resistance sampled in the DC excitation method is marked in Figure S5.

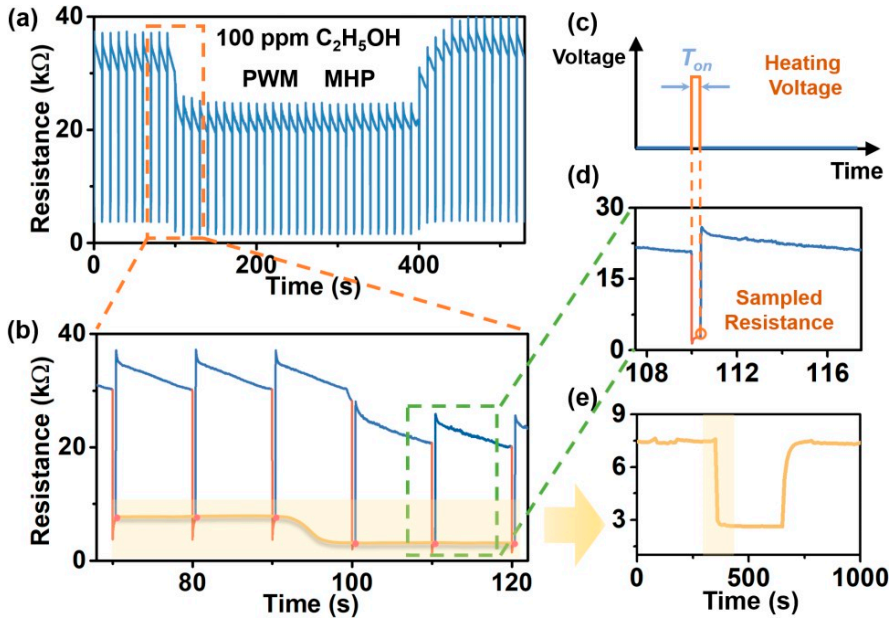

Figure 6. Resistance sampling under PWM excitation method. (**a**) Detailed resistance value of the response–recovery curve on exposure to 100 ppm ethanol. (**b**) Enlarged view of the response stage on ethanol vapor. (**c**) Heating voltage in one cycle under PWM excitation method. (**d**) Detailed resistance value under single heating cycle. (**e**) Response–recovery curve on exposure to 100 ppm ethanol.

Figure 7 illustrates the sensing behavior of the proposed gas sensors under different circumstances, where the ceramic tube gas sensor and the MHP sensor using the DC excitation method were used as comparisons. The corresponding operating resistance curves are pictured in Figure 7a–c, providing an overview of the sensors' performance. In addition, the response–recovery curves on exposure to 100 ppm ethanol vapor are shown in Figure 7d–f. Additionally, the calculated response and recovery times under these circumstances are pictured in Figure S4. Figure 7g provides the response curve for lower concentrations (0–50 ppm) of ethanol, proving the sensor's sensing ability for low concentrations of ethanol under the PWM excitation method. Additionally, the corresponding measurement of the ceramic tube and MHP under DC excitation is given in Figure S6 as a comparison. These results indicate that the MHP sensor showed a similar response (defined by Response = R_{air}/R_{gas}) in DC and PWM excitation modes, and a detailed comparison of the sensing performance is provided in Table 1.

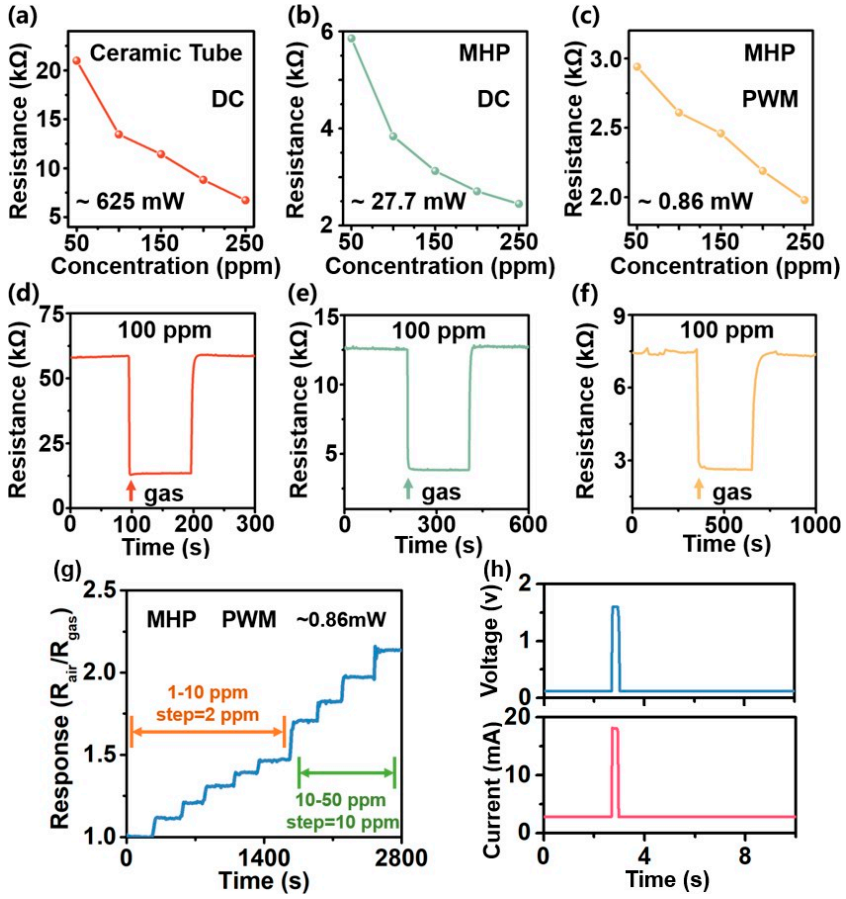

Figure 7. Operating resistance curve under (**a**) DC heating on ceramic substrate (**b**) DC heating on MHP and (**c**) PWM heating on MHP. (**d**–**f**) Response–recovery curve on exposure to 100 ppm etha-ol. (**g**) Response to 0–50 ppm ethanol at 1 mW. (**h**) Measured voltage and current value for power consumption.

Table 1. Sensing performance of the sensor under different heating conditions.

Heating Condition	Response (100 ppm C_2H_5OH)	Response Time	Heating Power
Ceramic tube (DC)	4.29	2 s	625 mW
MHP (DC)	3.21	3 s	27.7 mW
MHP (PWM)	3.03	$1 \times T = 10$ s	0.86 mW

Additionally, the baseline resistance value after stabilization under the pulse heating method was measured (Figure S7). Additionally, the dynamic response of four cycles of 50 ppm of ethanol is given in Figure S8 (the MHP sensor under the PWM signal), proving the stable sensing performance under the periodic temperature rise and fall cycles. The real-time heating power was measured at 0.86 mW using the sampled voltage (v) and current (mA) values, which are given in Figure 7h. The data above provide a comprehensive analysis of the proposed gas sensors' sensing behavior. These results have proved the effectiveness of detecting ethanol vapor at both high and low concentrations using the PWM excitation method, which can remarkably cut down the sensor's heating power. In addition, we compared the sensing performance for the detection of formaldehyde. Additionally, the results in Figure S9 prove the universality of the proposed method in the detection of reducing gases.

3.3. Sensing Mechanism

The possible reason that the suggested MHP sensors could function with the PWM excitation method without the necessity of a continuous high temperature is studied as follows. The chemical condition and reactions are determined by the temperature of the material's surface provided by the microheater, which is regulated by the heating voltage signal.

As modeled in Figure 8, the sensor undergoes the following transition with the temperature change in one heating cycle. Before the heating stage (State I), the sensing material absorbs the target gas molecules and dissociative oxygen at room temperature; the absorbed air layer could prevent the formation of the chemically absorbed target gas molecules. In the meantime, the primary existing form of reactive oxygen is O2−, which appears with low activity in the reaction between the chemical-absorbed molecules. These effects lead to a low charge carrier concentration in the MOS material, and the sensor appears with high resistance.

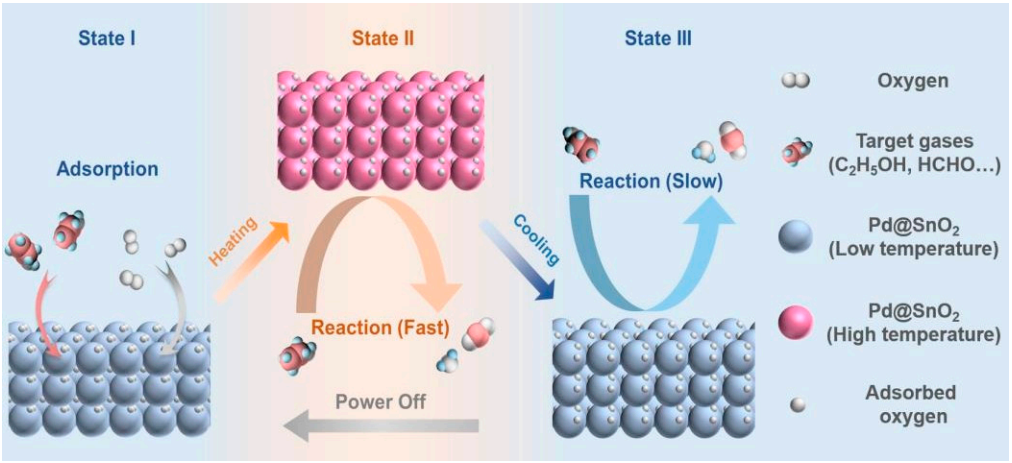

Figure 8. Schematic diagram of sensing mechanism of the MHP gas sensors under PWM excitation method.

After the heating voltage is switched to U_{on} (State II), the reactive oxygen in the sensing layer can convert to O_2^- ($O_2^- + e^- \rightarrow 2O^-$) owning to the energy provided by the high temperature (150~400 °C) [28–31]. This form of absorbed oxygen has a high chemical activity, which facilitates its reaction with absorbed target gases. The charge carrier released by the reaction between reactive oxygen and molecules of the target gases reduces the sensor's resistance [32]. Additionally, the measured resistance value at the end of the U_{on} is used as the output signal in gas detection. At the same time, a high temperature could work as an advantage in the gas desorption process, ensuring the release of reaction residuals such as water and carbon dioxide molecules from the sensing layer.

After the excitation of the heating voltage (State III), the MHP begins to cool down, causing an instantaneous low temperature in the sensing material. In that case, the chemical absorbed oxygen in the sensing layer, which is mainly O^-, is frozen on the sensing material because the temperature cannot provide enough energy for the chemical desorption process. Therefore, the reaction between the target gases and the reactive oxygen can continue even though the surface of the sensing material has returned to room temperature, owing to the delayed existence of the absorbed oxygen in the sensing layer. Therefore, during the response phase of gas detection, an obvious change in the sampled resistance values could be observed in adjacent cycles at the end of each U_{on} (Supporting information). In addition, the physical absorption process under a low temperature cannot be ignored the diffused target gases and oxygen accumulated in the sensing layer provide reactants for the successive chemisorption and redox reaction in the next cycle's *Ton*. These above processes illustrate the reason that MHP gas sensors could show a clear response in gas detection under pulse heating mode with an extremely short heating duration, and these operating characteristics facilitate the realization of ultra-low power consumption. This information can be used to further optimize the design and performance of the sensors for a wide range of gas-sensing applications.

4. Conclusions

In this paper, an ultra-low power consumption method for MOS gas sensors was implemented based on a Si substrate with MHP. The PWM heating voltage was used to realize the periodic high temperature of the MHP's surface, along with a sampling system to measure the resistance of the gas-sensing material at the end of each heating period. The parameters of the PWM heating voltage were acquired by studying the MHP's properties in experiments. Additionally, Pd-doped SnO_2 was synthesized through a sol-gel method, which was used as the sensing material in ethanol vapor detection. The sensing performances of the fabricated sensors with different heating methods were explored in the measurements. The results indicate that traditional MOS materials could work fine using the proposed method while reducing power consumption to around 1 mW. Moreover, the sensing mechanism based on the MOS material's transition with temperature was elaborated to explain the reason that MHP gas sensors could work under a pulse heating method. Therefore, the implementation of this work provides a new strategy for realizing ultra-low power MEMS gas sensing, enabling their application in portable devices with higher energy-saving requirements.

Supplementary Materials: The following supporting information can be downloaded at: https://www.mdpi.com/article/10.3390/chemosensors11040236/s1, Figure S1. The peripheral circuit connected to DAC output pin; Figure S2. The photo under camera and microscope (×50 and ×100); Figure S3. The response—temperature curve to 500 ppm ethanol; Figure S4. Response and recovery time under (a) DC heating on ceramic substrate, (b) DC heating on MHP, and (c) PWM heating on MHP. Figure S5. The resistance variation in the MHP sensor after the application of heating voltage. Figure S6. Response to 0–50 ppm ethanol under (a) DC heating on ceramic substrate (b) DC heating on MHP. Figure S7. The MHP sensor's baseline resistance value under the PWM signal. Figure S8. The dynamic response variation in four cycles of the MHP sensor exposed to 50 ppm ethanol (under PWM signal). Figure S9. The dynamic response variation of three cycles of the MHP sensor exposed to 100 ppm formaldehyde using (a) DC (b) PWM signal.

Author Contributions: Writing—original draft: Y.B. and H.M.; investigation: Y.B.; supervision: F.Z.; software: J.H.; methodology: T.Z. (Tingting Zhou); formal analysis: H.M.; validation: F.Z., J.H. and T.Z. (Tingting Zhou); project administration: T.Z. (Tong Zhang); writing—review and editing: T.Z. (Tong Zhang). All authors have read and agreed to the published version of the manuscript.

Funding: This work is supported by the National Key R&D Program of China (2021YFB3200402), Natural Science Foundation Committee (NSFC, Grant Nos. 62020106006 and 62101208) and Graduate Innovation Fund of Jilin University (2022076).

Institutional Review Board Statement: Not applicable.

Informed Consent Statement: Not applicable.

Data Availability Statement: Not applicable.

Conflicts of Interest: The authors declare no conflict of interest.

References

1. Siregar, J.; Septiani, N.L.W.; Abrori, S.A.; Sebayang, K.; Irzaman; Fahmi, M.Z.; Humaidi, S.; Sembiring, T.; Sembiring, K.; Yuliarto, B. Review—A Pollutant Gas Sensor Based on Fe_3O_4 Nanostructures: A Review. *J. Electrochem. Soc.* **2021**, *168*, 027510. [CrossRef]
2. Popa, D.; Udrea, F. Towards Integrated Mid-Infrared Gas Sensors. *Sensors* **2019**, *19*, 2076. [CrossRef] [PubMed]
3. Wang, T.; Huang, D.; Yang, Z.; Xu, S.; He, G.; Li, X.; Hu, N.; Yin, G.; He, D.; Zhang, L. A Review on Graphene-Based Gas/Vapor Sensors with Unique Properties and Potential Applications. *Nano-Micro Lett.* **2016**, *8*, 95–119. [CrossRef] [PubMed]
4. Mirzaei, A.; Kim, J.-H.; Kim, H.W.; Kim, S.S. Resistive-based gas sensors for detection of benzene, toluene and xylene (BTX) gases: A review. *J. Mater. Chem. C* **2018**, *6*, 4342–4370. [CrossRef]
5. Ghaderahmadi, S.; Kamkar, M.; Tasnim, N.; Arjmand, M.; Hoorfar, M. A review of low-temperature H_2S gas sensors: Fabrication and mechanism. *N. J. Chem.* **2021**, *45*, 17727–17752. [CrossRef]
6. Tan, H.M.; Manh Hung, C.; Ngoc, T.M.; Nguyen, H.; Duc Hoa, N.; Van Duy, N.; Hieu, N.V. Novel Self-Heated Gas Sensors Using on-Chip Networked Nanowires with Ultralow Power Consumption. *ACS Appl. Mater. Interfaces* **2017**, *9*, 6153–6162. [CrossRef]
7. Sankar Ganesh, R.; Durgadevi, E.; Navaneethan, M.; Patil, V.L.; Ponnusamy, S.; Muthamizhchelvan, C.; Kawasaki, S.; Patil, P.S.; Hayakawa, Y. Low temperature ammonia gas sensor based on Mn-doped ZnO nanoparticle decorated microspheres. *J. Alloys Compd.* **2017**, *721*, 182–190. [CrossRef]
8. Zhao, J.; Hu, M.; Liang, Y.; Li, Q.; Zhang, X.; Wang, Z. A room temperature sub-ppm NO_2 gas sensor based on WO_3 hollow spheres. *N. J. Chem.* **2020**, *44*, 5064–5070. [CrossRef]
9. Li, Z.; Wang, J.; Wang, N.; Yan, S.; Liu, W.; Fu, Y.Q.; Wang, Z. Hydrothermal synthesis of hierarchically flower-like CuO nanostructures with porous nanosheets for excellent H_2S sensing. *J. Alloys Compd.* **2017**, *725*, 1136–1143. [CrossRef]
10. Wang, Y.; Zhao, Z.; Sun, Y.; Li, P.; Ji, J.; Chen, Y.; Zhang, W.; Hu, J. Fabrication and gas sensing properties of Au-loaded SnO_2 composite nanoparticles for highly sensitive hydrogen detection. *Sens. Actuators B Chem.* **2017**, *240*, 664–673. [CrossRef]
11. Ju, D.; Xu, H.; Qiu, Z.; Guo, J.; Zhang, J.; Cao, B. Highly sensitive and selective triethylamine-sensing properties of nanosheets directly grown on ceramic tube by forming NiO/ZnO PN heterojunction. *Sens. Actuators B Chem.* **2014**, *200*, 288–296. [CrossRef]
12. Sharma, S.; Madou, M. A new approach to gas sensing with nanotechnology. *Philos. Trans. R. Soc. A Math. Phys. Eng. Sci.* **2012**, *370*, 2448–2473. [CrossRef] [PubMed]
13. Du, H.; Yang, W.; Yi, W.; Sun, Y.; Yu, N.; Wang, J. Oxygen-Plasma-Assisted Enhanced Acetone-Sensing Properties of ZnO Nanofibers by Electrospinning. *ACS Appl. Mater. Interfaces* **2020**, *12*, 23084–23093. [CrossRef]
14. Jian, J.; Guo, X.; Lin, L.; Cai, Q.; Cheng, J.; Li, J. Gas-sensing characteristics of dielectrophoretically assembled composite film of oxygen plasma-treated SWCNTs and PEDOT/PSS polymer. *Sens. Actuators B Chem.* **2013**, *178*, 279–288. [CrossRef]
15. Yuan, Z.; Yang, F.; Meng, F. Research Progress on Coating of Sensitive Materials for Micro-Hotplate Gas Sensor. *Micromachines* **2022**, *13*, 491. [CrossRef]
16. Li, M.; Luo, W.; Liu, X.; Niu, G.; Wang, F. Wafer-Level Patterning of SnO Nanosheets for MEMS Gas Sensors. *IEEE Electron Device Lett.* **2022**, *43*, 1981–1984. [CrossRef]
17. Xu, L.; Li, T.; Gao, X.; Wang, Y. Development of a Reliable Micro-Hotplate with Low Power Consumption. *IEEE Sens. J.* **2011**, *11*, 913–919. [CrossRef]
18. Hasan, M.N.; Sahlan, S.; Osman, K.; Mohamed Ali, M.S. Energy Harvesters for Wearable Electronics and Biomedical Devices. *Adv. Mater. Technol.* **2021**, *6*, 2000771. [CrossRef]
19. Prasad, M.; Dutta, P.S. Development of micro-hotplate and its reliability for gas sensing applications. *Appl. Phys. A* **2018**, *124*, 788. [CrossRef]
20. Liu, Q.; Yao, J.; Wu, Y.; Wang, Y.; Ding, G. Two operating modes of palladium film hydrogen sensor based on suspended micro hotplate. *Int. J. Hydrog. Energy* **2019**, *44*, 11259–11265. [CrossRef]
21. Liu, L.; Wang, Y.; Sun, F.; Dai, Y.; Wang, S.; Bai, Y.; Li, L.; Li, T.; Zhang, T.; Qin, S. "Top-down" and "bottom-up" strategies for wafer scaled miniaturized gas sensors design and fabrication. *Microsyst. Nanoeng.* **2020**, *6*, 31. [CrossRef] [PubMed]
22. Xie, D.; Chen, D.; Peng, S.; Yang, Y.; Xu, L.; Wu, F. A Low Power Cantilever-Based Metal Oxide Semiconductor Gas Sensor. *IEEE Electron Device Lett.* **2019**, *40*, 1178–1181. [CrossRef]
23. Jeong, Y.J.; Koo, W.-T.; Jang, J.-S.; Kim, D.-H.; Kim, M.-H.; Kim, I.-D. Nanoscale PtO_2 Catalysts-Loaded SnO_2 Multichannel Nanofibers toward Highly Sensitive Acetone Sensor. *ACS Appl. Mater. Interfaces* **2018**, *10*, 2016–2025. [CrossRef] [PubMed]
24. van den Broek, J.; Güntner, A.T.; Pratsinis, S.E. Highly Selective and Rapid Breath Isoprene Sensing Enabled by Activated Alumina Filter. *ACS Sens.* **2018**, *3*, 677–683. [CrossRef]
25. Duan, P.; Xiao, H.; Wang, Z.; Peng, Q.; Jin, K.; Sun, J. Hydrogen sensing properties of Pd/SnO_2 nano-spherical composites under UV enhancement. *Sens. Actuators B Chem.* **2021**, *346*, 130557. [CrossRef]
26. Lu, S.; Zhang, Y.; Liu, J.; Li, H.-Y.; Hu, Z.; Luo, X.; Gao, N.; Zhang, B.; Jiang, J.; Zhong, A.; et al. Sensitive H_2 gas sensors based on SnO_2 nanowires. *Sens. Actuators B Chem.* **2021**, *345*, 130334. [CrossRef]

27. Li, G.; Wang, X.; Yan, L.; Wang, Y.; Zhang, Z.; Xu, J. PdPt Bimetal-Functionalized SnO_2 Nanosheets: Controllable Synthesis and its Dual Selectivity for Detection of Carbon Monoxide and Methane. *ACS Appl. Mater. Interfaces* **2019**, *11*, 26116–26126. [CrossRef]
28. Suematsu, K.; Harano, W.; Oyama, T.; Shin, Y.; Watanabe, K.; Shimanoe, K. Pulse-Driven Semiconductor Gas Sensors Toward ppt Level Toluene Detection. *Anal. Chem.* **2018**, *90*, 11219–11223. [CrossRef] [PubMed]
29. Suematsu, K.; Oyama, T.; Mizukami, W.; Hiroyama, Y.; Watanabe, K.; Shimanoe, K. Selective Detection of Toluene Using Pulse-Driven SnO_2 Micro Gas Sensors. *ACS Appl. Electron. Mater.* **2020**, *2*, 2913–2920. [CrossRef]
30. Ji, H.; Zeng, W.; Li, Y. Gas sensing mechanisms of metal oxide semiconductors: A focus review. *Nanoscale* **2019**, *11*, 22664–22684. [CrossRef]
31. Yamazoe, N.; Suematsu, K.; Shimanoe, K. Extension of receptor function theory to include two types of adsorbed oxygen for oxide semiconductor gas sensors. *Sens. Actuators B Chem.* **2012**, *163*, 128–135. [CrossRef]
32. Lei, T.; Rao, Z.; Zhang, S.; Cai, S.; Xie, C. The irreversible R-T curves of metal oxide gas sensor under programmed temperature cycle. *Sens. Actuators B Chem.* **2016**, *235*, 481–491. [CrossRef]